

# Novel Strategies for Fine-Segmented Low Gain Avalanche Diodes

G. Paternoster<sup>a,b,\*</sup>, G. Borghi<sup>a,b</sup>, R. Arcidiacono<sup>c,f</sup>, M. Boscardin<sup>a,b</sup>, N. Cartiglia<sup>c</sup>, M. Centis Vignali<sup>a</sup>, G. F. Dalla Betta<sup>d,b</sup>, M. Ferrero<sup>f</sup>, F. Ficorella<sup>a,b</sup>, M. Mandurrino<sup>c</sup>, L. Pancheri<sup>d,b</sup>, F. Siviero<sup>c,e</sup>, V. Sola<sup>c,e</sup>, M. Tornago<sup>c,e</sup>

<sup>a</sup>*Fondazione Bruno Kessler, Centre of Materials and Microsystems, Trento, ITALY.*

<sup>b</sup>*TIFPA-INFN, via Sommarive 18, 38123, Trento, Italy*

<sup>c</sup>*INFN, Torino, Italy*

<sup>d</sup>*Università di Trento, Trento, Italy*

<sup>e</sup>*Università di Torino, Torino, Italy*

<sup>f</sup>*Università del Piemonte Orientale, Italy*

---

## Abstract

Low Gain Avalanche Diodes (LGADs) are now considered a viable solution for 4D-tracking thanks to their excellent time resolution and good resistance to high radiation fluence. However, the currently available LGAD technology is well suited only for applications that require coarse space precision, pixels with pitch in the range 500  $\mu\text{m}$  - 1 mm, due to the presence of a no-gain region between adjacent pixels of about 50  $\mu\text{m}$ , in which the gain is completely suppressed. In this paper, we will discuss the segmentation issues in the standard LGAD technology and we will present two new segmentation strategies aimed at producing LGADs with high spatial resolution and high fill factor. The first presented design is the so-called Trench-Isolated LGAD (TI-LGAD). Here, the pixel isolation is provided by trenches, physically etched in the silicon and then filled with silicon oxide. The second design is the Resistive AC-coupled Silicon Detector (RSD), an evolution of LGADs, where the segmentation is obtained by means of AC-coupled electrodes.

Prototypes of both designs have been produced at FBK and characterized at the Laboratories for Innovative Silicon Sensors (INFN and University of Turin) by means of a laser setup to estimate the space resolution and the fill factor. The functional characterization shows that both technologies yield fully working small pixel LGADs (down to 50  $\mu\text{m}$ ), providing the first examples of sensors able to concurrently measure space and time with excellent precision.

*Keywords:* Silicon sensors, fast detectors, LGAD, TI-LGAD, RSD, AC-LGAD, 4D-tracking

*2010 MSC:* 00-01, 99-00

---

\*Corresponding author

*Email address:* [paternoster@fbk.eu](mailto:paternoster@fbk.eu) (G. Paternoster)

## 1. Introduction

Low Gain Avalanche Diodes (LGADs) are silicon sensors based on p-n junction and provided with an internal signal amplification mechanism (gain) [1]. The internal structure is similar to that of silicon Avalanche Photodiodes (APDs), but the gain is much lower ( $\mathcal{O}(10)$  with respect to  $\mathcal{O}(1000)$  of APD). The combination of low gain and thin active silicon substrates already made LGADs a viable choice for those applications that requires good time resolution and high resistance to radiation, as in the case of detectors for High Energy Physics (HEP) experiments [2, 3].

Another important feature of LGADs is the possibility to arrange the single diodes in large-area segmented sensors (pixel arrays or strips), which are able to provide information on both time and position of interaction of the detected particles.

The latter aspect is a key enabling feature for the so-called “4-dimensional (4D) tracking”, which requires a concurrently  $\mathcal{O}(10)$  ps time resolution and a  $\mathcal{O}(10)$   $\mu\text{m}$  space resolution in Minimum Ionizing Particles (MIP) detection [4]. A first example of a LGAD designed for 4D tracking are the Ultra Fast Silicon Detectors (UFSDs), which have been developed for the High Luminosity (HL) upgrade of LHC. These sensors reach the required specifications in terms of radiation hardness, space and time resolution [5, 6, 7]. However, additional development has to be done to meet the requests of the next generation of HEP experiments and those of other applications, such as x-ray imaging or ion tracking in devices for medical applications (hadrontherapy) [8, 9].

The current R&D activities on LGADs are focused on three different goals, interconnected with each other: (i) improvement of the time resolution; (ii) increase of the radiation hardness (fluences above  $10^{15}$  neq/cm<sup>2</sup>); (iii) improvement of the spatial resolution. This paper is focused on the latter task, which has been also the least investigated by the scientific community in the past few years.

In the following section, we discuss the current state-of-the-art technology for segmenting LGADs, pointing out its limiting factors. In section 3 we introduce two new segmentation strategies to develop fine-pitch LGADs. The first proposed scheme is the so-called Trench-Isolated LGAD (TI-LGAD), while the second is the Resistive AC-coupled Silicon Detector (RSD). In both cases, experimental characterization will be shown and discussed.

## 2. Segmentation of Standard LGAD

A schematic drawing of the internal structure of a n-in-p diode array (PIN) and of an LGAD is shown in Fig. 1. PIN diodes are usually based on a deep and segmented n<sup>+</sup> junction on a high-resistivity p-type substrate. In these sensors, the electrical isolation among pixels is usually provided by a p-doped region (p-stop) that surrounds each pixel.

Segmented silicon detectors with internal multiplication need to face additional hurdles with respect to conventional silicon sensors. Indeed, in LGADs, the basic multiplying structure is usually based on a shallow n<sup>+</sup> junction and on a deep p-type multiplication layer below the junction. This doping region, also named “gain layer”, locally increases the electric field to values higher than the impact-ionization threshold (about  $2 \times 10^5$  V cm<sup>-1</sup>), enabling the mechanism responsible of charge multiplication. When segmented, beside the standard p-stop isolation region, these multiplying junctions require a complex design of the border region, in order to avoid undesired regions with high

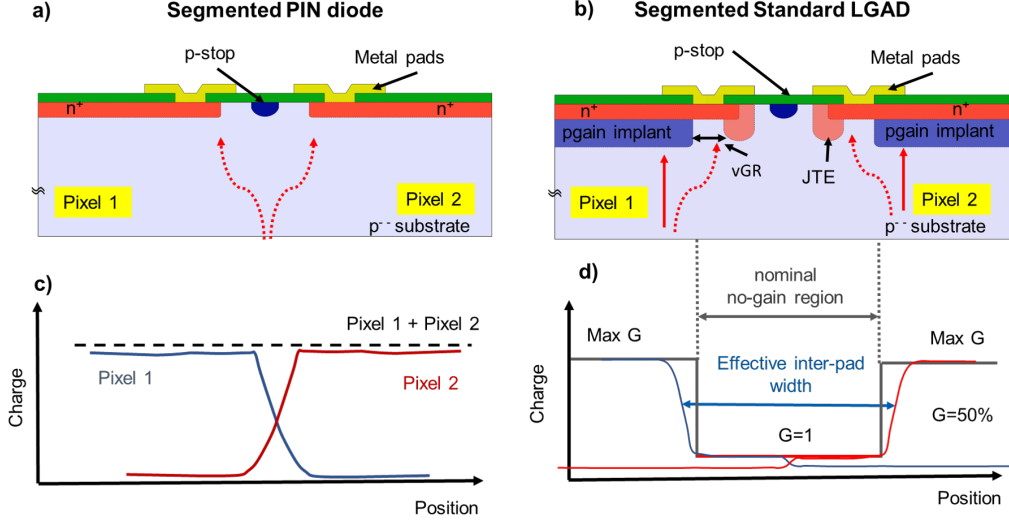


Figure 1: Schematic drawings of a segmented PIN diode (a) and of a segmented LGAD (b). A sketch of the generated signals from PIN and LGAD are reported in c) and d), respectively.

45 electric field [10]. Therefore, an additional n-type region, named Junction Termination  
 46 Extension (JTE), is typically included at the  $n^+$  periphery, with the role to control the  
 47 junction curvature and reduce the electric field at the border. The gain layer is also  
 48 interrupted below the JTE and at the p-stop regions, also in this case to reduce the  
 49 electric field and prevent premature breakdown at the pixel edge (or edge-breakdown).  
 50 To further control the edge electric field, the gain layer is also kept at a certain distance  
 51 from the edge of the JTE, in order to create the so-called virtual guard ring (vGR).

52 As a consequence, a relatively wide gap is created between the gain layers of two  
 53 adjacent pixels: this gap is called “no-gain” region, since the ionization produced by  
 54 particles impinging in that area is not multiplied. This is represented in Fig. 1 c) and  
 55 d), where the signal produced by a particle as a function of the impinging position is  
 56 represented for a PIN and an LGAD detector, respectively. In the case of a PIN diode, the  
 57 charges generated by a particle interacting at the pixel periphery are typically shared  
 58 among neighboring pixels and the sum of the signals from all the involved pixels is a  
 59 constant. In the LGAD case, instead, the signal is multiplied only in the pixel core  
 60 region and not at the pixel periphery, since, in this region, the generated charges are  
 61 collected by the JTE and do not cross the gain layer. As a consequence, the total signal  
 62 is not constant but varies from a maximum value, corresponding to the nominal gain  
 63 ( $G$ ), to the minimum  $G = 1$ . We can define the fill factor (FF) of the LGAD pixel as

$$FF = \frac{\text{pixel area with signal multiplication}}{\text{total pixel area}}. \quad (1)$$

64 The nominal width of the no-gain region depends on both technological and physical  
 65 limitations since (i) the technological constraints of the fabrication process put a limit on  
 66 the minimum achievable feature size and on the alignment precision which is achievable

67 among different structures; (ii) a too small gap between n-doped regions and p-stop  
 68 generates high electric fields that would lead to premature edge-breakdown and “pop-  
 69 corn” noise [11].

70 In the past few years, several efforts have been made to reduce the width of the no-  
 71 gain region, by optimizing both the fabrication technology and the sensor layout. Table  
 72 1 reports the evolution of the nominal no-gain width in the different batches produced  
 73 at FBK in the last few years. In the first batch, the no-gain width was 210  $\mu\text{m}$  and it  
 74 has been reduced in the following productions down to 20.5  $\mu\text{m}$ , a value that could be  
 considered the state-of-the-art of the standard FBK-LGAD technology.

Table 1: Evolution of the no-gain width in FBK productions

Batch	Year	No-gain width
UFSD 1	2016	210 $\mu\text{m}$
UFSD 2	2017	66 $\mu\text{m}$
UFSD 3 - Safe	2018	31 $\mu\text{m}$
UFSD 3 - Intermediate	2018	20.5 $\mu\text{m}$

75

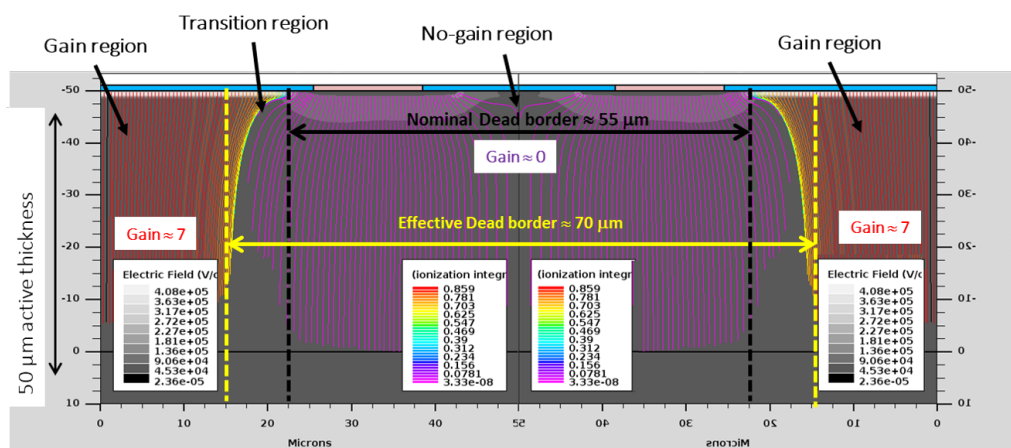


Figure 2: TCAD Simulation of LGAD sensor. The electric field intensity at the border region between two pixel is represented by the gray-scale map. Solid lines show the carriers path through the junction, while the lines color represents the ionization integral value.

76 An additional factor that could affect the FF of STD-LGADs is the uneven electric  
 77 field at the pixel border, which could lead to spatial non-uniformity in the charge carriers  
 78 collection and multiplication.

79 In order to understand this effect, TCAD simulations (Silvaco simulation tools [12])  
 80 have been exploited to investigate the collection mechanisms at the border region of the  
 81 pixel. Fig. 2 represents the electric field (gray scale map) of a segmented LGAD (same  
 82 structure represented in Fig. 1), while the solid lines represent the carrier drift path lines,  
 83 and the lines color is the ionization integral along that carrier path. The bias voltage is  
 84 about 200 V, and the gain at the pixel core is about 7. The ionization integral reaches a

85 plateau (red lines, corresponding to the maximum gain) in the pixel core region, while it  
 86 is almost zero in the no-gain region (purple lines). Moreover, it is possible to identify a  
 87 third region, indicated as “transition region”, where the carriers, even though generated  
 88 in the nominal gain region, are collected by the JTE and are only partially multiplied.  
 89 The transition region reduces the effective FF of the pixel and plays a very important role  
 90 in the case of small pixels, or when the pixel area is comparable to substrate thickness  
 91 (typically  $50\ \mu\text{m}$  in thin LGAD). It is possible to define the “effective inter-pixel width”  
 92 as the distance between the two locations in adjacent pixels where the generated signals  
 93 are equal to 50% of the maximum signal value, as represented in Fig. 1d. The width of  
 94 the transition region could depend on multiple factors: (i) bias voltage, (ii) generation  
 95 depth of the charge carriers, (iii) doping lateral diffusion, and (iv) doping concentration  
 96 of the gain layer. An accurate simulation campaign of these effects is currently under  
 97 way.

98 An experimental measurement of the signal variation at the pixel border of STD-  
 99 LGAD is reported in Fig. 3. The measurement was performed at the Laboratories for  
 100 Innovative Silicon Sensors of the INFN and University of Turin, using the Transient  
 101 Current Technique (TCT) setup described in [Ferrero 2020]. In this setup, a focused  
 102  $1064\ \text{nm}$  laser (spot size of  $\sim 10\ \mu\text{m}$ ) is used to simulate the passage of a MIP in different  
 103 position of the sensors pixels, directly measuring the sensor response in the inter-pad  
 104 region.

105 The sensor in Fig. 3 is a STD-LGAD from FBK-UFSD3 batch production with a  
 106 nominal no-gain region of  $31\ \mu\text{m}$ . It is worth noting that the measured inter-pad width  
 107 is  $38\ \mu\text{m}$ , slightly wider than the nominal one, as suggested by TCAD simulations.

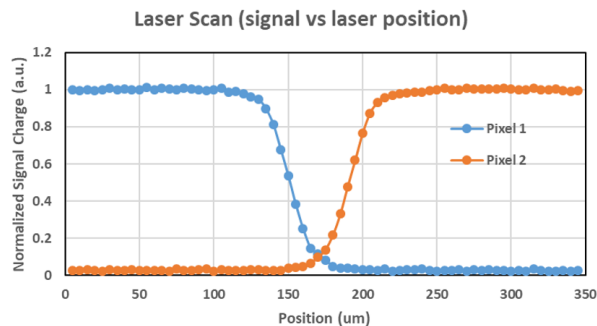


Figure 3: Signal charge vs position of the laser, scanning the inter-pad region (represented in the inset) of a STD-LGAD with a nominal no-gain region of  $31\ \mu\text{m}$ .

### 108 3. Novel Segmentation Schemes

109 In order to reduce the width of the no-gain region, novel detectors schemes have been  
 110 recently proposed. Fig. 4 represents four different segmentation schemes:

- 111 a) Standard LGAD;
- 112 b) Double-sided LGAD (or inverted LGAD, i-LGAD);
- 113 c) Trench-Isolated LGAD (TI-LGAD);

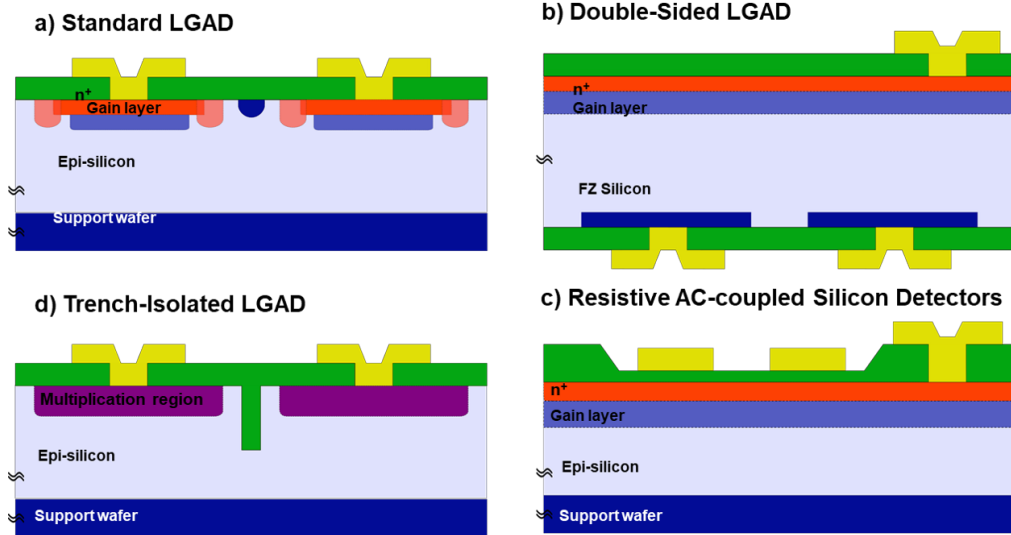


Figure 4: Schematic drawings of different segmentation technologies for LGAD: a) Standard segmentation; b) Double-Sided LGAD; c) Trench-Isolated LGAD; d) Resistive AC-coupled Silicon Detectors;

114 d) Resistive AC-Coupled Silicon Detectors (RSD, or AC-LGAD).

115 The Standard LGAD Segmentation has been described in the previous section. In  
 116 Double-sided LGADs (or inverted-LGAD), the junction and the gain layer are not-  
 117 segmented and the read-out segmentation is transferred on the back side of the sensor,  
 118 where  $p^+$  contacts are defined [13, 2]. These sensors are typically produced on thick  
 119 (about  $300\ \mu\text{m}$ ) silicon wafers with a double-sided fabrication process. Using this inte-  
 120 gration scheme, it is possible to produce pixels with 100% FF and a uniform response  
 121 along the sensitive region [14].

122 The third technology is the so-called Trench-Isolated LGAD (TI-LGAD). In this new  
 123 design, the electrical isolation among pixels is obtained by means of trenches, physically  
 124 etched in the silicon and filled with silicon oxide. Such an isolation scheme makes pos-  
 125 sible to reduce the no-gain width down to a few microns without affecting the detector  
 126 performance.

127 The fourth scheme represents the Resistive AC-coupled Silicon Detectors, in which  
 128 the multiplying junction is created using a resistive  $n^+$ -layer. In these sensors, the  $n^+$ -  
 129 layer and gain layer are not segmented and the read-out segmentation is provided by  
 130 metal pads that are AC-coupled to the resistive  $n^+$ -layer via a thin dielectric layer.

131 Both RSD and TI-LGADs technologies will be presented in the following parts of this  
 132 section.

### 133 3.1. Trench-Isolated LGAD

134 An alternative technological solution for the isolation of adjacent components in an  
 135 integrated circuit device is the so-called Deep Trench Isolation (DTI) technique. This  
 136 technology consists in the etching of a pattern of trenches in the silicon substrate. The  
 137 trenches are subsequently filled with dielectric materials, such as silicon dioxide.

138 In the past years, DTI has been extensively used for pixel isolation in CMOS image  
 139 sensors [15], as well as in other avalanche detectors, such as Silicon Photomultipliers  
 140 (SiPM) [16]. In particular, in SiPMs, DTI are also used as an optical barrier to reduce  
 141 the internal optical cross-talk among adjacent pixels [17].

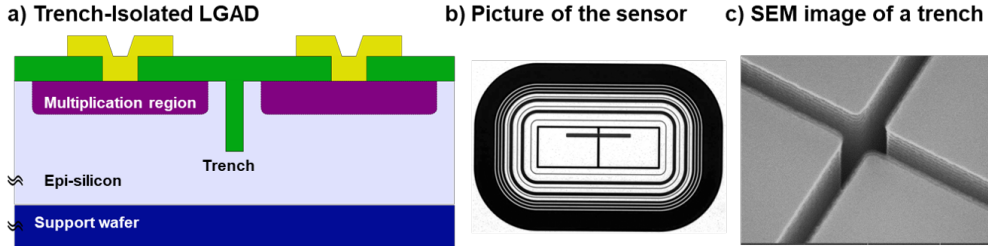


Figure 5: Schematic drawing of TI-LGAD (a); Picture of a  $1 \times 2$  pads array produced at FBK (b); SEM image of a trench before filling (c).

142 Trench-Isolated LGADs exploit DTI technology to provide electrical isolation among  
 143 the pixels of a segmented LGAD. A schematic cross sectional view of TI-LGAD is re-  
 144 ported in Fig. 5a. While the multiplying junction scheme ( $n^+ - p^+ - p^- - p^+$ ) remains the  
 145 same as STD-LGADs, all the junction termination and isolation structures (JTE and p-  
 146 stop) are here completely replaced with a single trench, that is less than  $1 \mu\text{m}$  wide. This  
 147 design offers a clear advantage in terms of reduction of the no-gain region between the  
 148 pixels and overcomes the technological limitations of the standard technology described  
 149 in the previous section.

150 The trench is etched in the silicon substrate during the fabrication process by means  
 151 of the Deep Reactive Ion Etching (DRIE) technique, which is able to produce submicron  
 152 trenches with high aspect ratio (up to  $20 : 1$ ). A Secondary Electron Microscope (SEM)  
 153 image of a trench after the etching process is shown in Fig. 5c. After the etching, the  
 154 trenches are filled with silicon dioxide to passivate the trench surface and to recover the  
 155 wafer planarity. The first production of TI-LGAD has been carried out at FBK in 2019:  
 156 a detailed description of these first prototypes and of their characterization can be found  
 157 in [18].

158 Preliminary TCAD simulations of these devices show that DTI is effective in reducing  
 159 the inter-pad width down to  $5 \mu\text{m}$ , a factor of five narrower than in state-of-the-art  
 160 standard LGADs, without affecting the detector performance [18].

161 The first produced samples have been characterized by means of a TCT setup and a  
 162 IR laser source (as described in the previous section). Fig. 6 reports in blue the signals  
 163 from two adjacent pads of the sensor in Fig. 5b (a  $1 \times 2$  pads array, with pad size equal  
 164 to  $275 \mu\text{m} \times 375 \mu\text{m}$ ). The laser has been swept along an optical window (an aperture in  
 165 the metal that crosses the two pixels) shown in Fig. 5b. The same measurement, carried  
 166 out on a STD-LGAD with a  $31 \mu\text{m}$  wide no-gain region, is plotted for reference. Both  
 167 the sensor are biased at  $200 - 250 \text{ V}$  in order to set the same gain for both the devices  
 168 ( $G = 15$ ).

169 The measured effective inter-pad width of the TI-LGAD sample is  $9 \mu\text{m}$ , much nar-  
 170 rower with respect to that of the STD-LGAD ( $38 \mu\text{m}$ ). In addition, since the two channels  
 171 are acquired simultaneously, it is possible to demonstrate that good electrical isolation

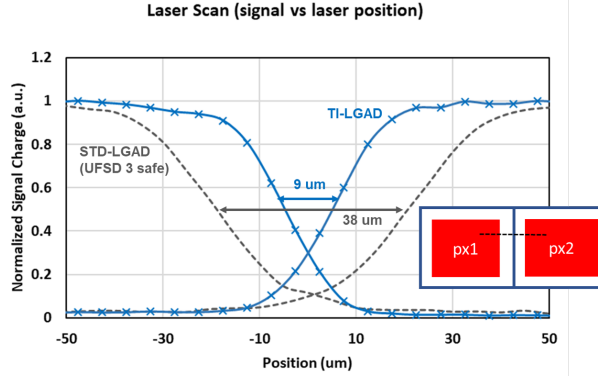


Figure 6: Laser scan through the inter-pad region (represented in the inset) of a TI-LGAD (blue line) and of a STD-LGAD (dark gray line).

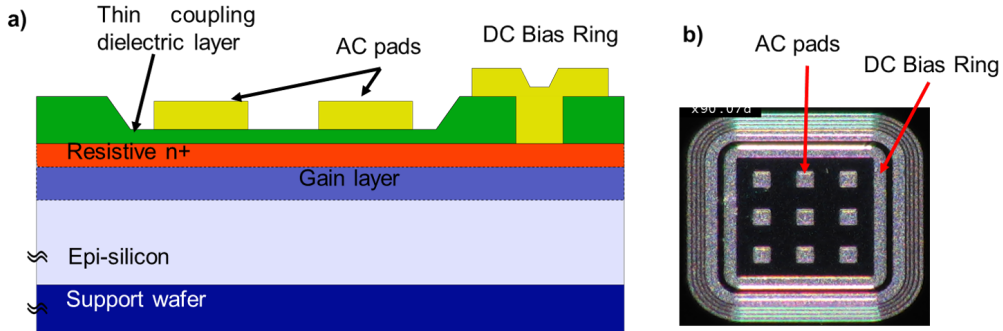


Figure 7: Schematic drawing of Resistive Silicon Detectors (a); Picture of a  $3 \times 3$  pads array produced at FBK (b).

172 between the pads is provided by the DTI technology.

173 With this improved technology it would be possible to produce segmented sensors  
 174 with  $100 \mu\text{m}$  or  $50 \mu\text{m}$  pitches with a remarkable FF of 83% and 67%, respectively.

### 175 3.2. Resistive AC-Coupled Silicon Detectors

176 A schematic cross section of an RSD sensor is reported in Fig. 7a, together with a  
 177 picture of a  $3 \times 3$  pad array produced at FBK (in Fig. 7b). This sensor is designed  
 178 following the principle of AC-coupled LGADs [19, 20], and optimized for 4D tracking  
 179 applications. The first production of these sensors has been carried out in the framework  
 180 of the RSD project, and presented in [21, 22].

181 In RSD, the  $n^+$  electrode and the gain layer extend along the entire sensor area,  
 182 without any patterning, thus providing a uniform gain through the sensor. The sensor  
 183 segmentation is achieved via AC-coupled metal pads that lie on a thin dielectric film,  
 184 while at the sensor periphery, the  $n^+$  electrode is connected to the ground via an ohmic  
 185 contact. The size of the AC metal pads determines the readout segmentation, while the  
 186 thickness of the dielectric layer determine the capacitive coupling between the pads and



187 the  $n^+$  layer. The sensors have been fabricated on silicon wafers with a  $50\ \mu\text{m}$  thick  
 188 epitaxial layer by means of a single-sided fabrication process, based on that used for the  
 189 production of STD-LGAD, and described in [7]. The major differences with respect to  
 190 the standard fabrication process regards the tuning of the  $n^+$  sheet resistance and the  
 191 local thinning of the top dielectric layer, aimed at finely selecting the capacitive coupling  
 192 between pads and the  $n^+$  electrode.

193 The signal formation process in RSD is substantially different from that of a standard  
 194 LGAD, as explained in [23]: in RSD, the signal at the readout pads is mainly induced after  
 195 that the charge carriers are collected at the  $n^+$  layer and the signal is propagating on the  
 196  $n^{++}$  layer, discharging to the ground. This mechanism is equivalent of the propagation  
 197 of a signal in a lossy transmission line. The main advantage of this readout scheme is  
 198 that the signal is shared among multiple pads, hundreds of microns far from the hit  
 199 point. The signal sharing through the resistive layer enhances the spatial resolution of  
 200 the sensor beyond the one achievable with segmented DC sensors (typically quoted as  
 201 pixel size/ $\sqrt{12}$ ), even at normal particle incidence.

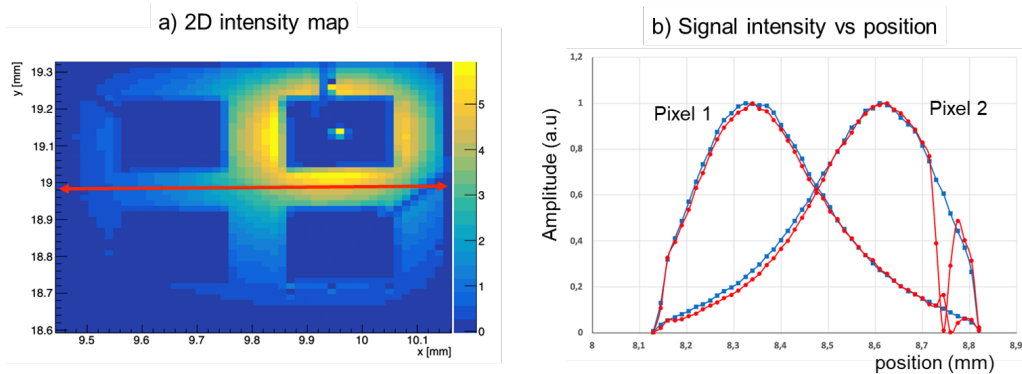


Figure 8: 2D maps of the intensity of the induced charge obtained with a TCT setup (a). The sensor is a  $2 \times 2$  pads array with  $300\ \mu\text{m}$  pitch. In b) the signal from two adjacent pixels acquired with a laser scan along the red line is reported.

202 Fig 8a reports a laser scan of the detector surface carried out with the same TCT  
 203 setup mentioned in Section 2. Each point of the image represents the intensity of the  
 204 signal generated on a single pad of a  $2 \times 2$  pixels sensor with  $300\ \mu\text{m}$  pitch. It is worth  
 205 noting that the signal intensity decreases radially with the distance from the pad. This  
 206 can be observed even better in Fig 8b, where the signal sharing between two neighboring  
 207 pixels is measured by means of a laser, scanning the sensor along the red line in Fig.  
 208 8a. It is important to stress that the sum of the signals from the two pixels is almost a  
 209 constant along the inter-pad region, an evidence that RSD acts as a 100% FF sensor.

210 To fully exploit the spatial resolution capabilities of this sensor, the position of an  
 211 hitting particles has to be calculated using a reconstruction algorithm that exploits the  
 212 signals in multiple pixels. A simple estimation of the hits' coordinates can be done  
 213 by using the amplitude-weighted centroid of the coordinates of four neighboring pads.  
 214 Preliminary results about the RSD spatial resolution are presented in [24], where a  
 215 resolution of  $20\ \mu\text{m}$  and  $6\ \mu\text{m}$  has been reported for sensors with  $200\ \mu\text{m}$  and  $100\ \mu\text{m}$  pitch,

216 respectively. The extremely good spatial resolution, obtained with a relatively coarse  
217 segmentation, leads to important advantages in terms of number of required readout  
218 channels.

#### 219 4. Conclusions

220 Latest developments of Low Gain avalanche detectors led this technology to a re-  
221 markable level of technological maturity, especially in particle tracking and timing ap-  
222 plications. However, the spatial resolution of these sensors is still limited by their coarse  
223 segmentation, due to the presence of a no-gain region between adjacent pixels of about  
224  $50\ \mu\text{m}$ . It has been demonstrated, also by means of TCAD simulations, as the standard  
225 segmentation approach of LGAD suffers from both intrinsic and technological limitations.

226 Several new segmentation strategies are currently being investigated to overcome  
227 these limitations. In particular, two new technologies have been discussed: TI-LGAD  
228 and RSD. The first one is able to reduce the inter-pad width to  $9\ \mu\text{m}$ , and in perspective  
229 down to  $5\ \mu\text{m}$ , enabling the possibility to design segmented sensors with fine pitch down  
230 to  $50\ \mu\text{m}$ . In the RSD technology instead, the improvement in the spatial resolution is  
231 reached by exploiting a completely different approach in the signal formation and read-  
232 out, which is based on AC-coupled electrodes. This readout mechanism enables charge  
233 sharing among the pixels, thus reaching a spatial resolution of  $6\ \mu\text{m}$  with a  $100\ \mu\text{m}$  pitch  
234 sensor.

235 Even if both these new technologies could be considered still at a first stage of develop-  
236 ment, they already shown very promising results that will be probably further enhanced  
237 in the next months thanks to improvements in the fabrication technology and in the  
238 sensor design.

#### 239 Acknowledgments

240 We thank our collaborators within RD50, ATLAS and CMS who participated in the  
241 development of UFSD. Part of this work has been financed by the European Union Hori-  
242 zon 2020 Research and Innovation funding program, under Grant Agreement no. 669529  
243 (ERC UFSD669529), by the Italian Ministero degli Affari Esteri, by INFN Gruppo V  
244 and by the Dipartimento di Eccellenza, University of Torino (ex L. 232/2016, art. 1, cc.  
245 314, 337). Some of the sensor productions presented in this work have been co-financed  
246 by FBK in the framework of the FBK-INFN agreement.

#### 247 References

- 248 [1] G. Pellegrini, P. Fernández-Martínez, M. Baselga, C. Fleta, D. Flores, V. Greco, S. Hidalgo,  
249 I. Mandić, G. Kramberger, D. Quirion, M. Ullan, Technology developments and first measurements  
250 of low gain avalanche detectors (lgad) for high energy physics applications, Nuclear Instruments  
251 and Methods in Physics Research Section A: Accelerators, Spectrometers, Detectors and Associated  
252 Equipment 765 (2014) 12 – 16. doi:<https://doi.org/10.1016/j.nima.2014.06.008>.
- 253 [2] G. Pellegrini, M. Baselga, M. Carulla, V. Fadeyev, P. Fernández-Martínez, M. F. García, D. Flores,  
254 Z. Galloway, C. Gallrapp, S. Hidalgo, Z. Liang, A. Merlos, M. Moll, D. Quirion, H. Sadrozinski,  
255 M. Stricker, I. Vila, Recent technological developments on lgad and ilgad detectors for tracking and  
256 timing applications, Nuclear Instruments and Methods in Physics Research Section A: Accelerators,  
257 Spectrometers, Detectors and Associated Equipment 831 (2016) 24 – 28. doi:<https://doi.org/10.1016/j.nima.2016.05.066>.

- 259 [3] H. F.-W. Sadrozinski, A. Seiden, N. Cartiglia, 4d tracking with ultra-fast silicon detectors, Reports  
 260 on Progress in Physics 81 (2) (2017) 026101. doi:10.1088/1361-6633/aa94d3.
- 261 [4] N. Cartiglia, R. Arcidiacono, B. Baldassarri, M. Boscardin, F. Cenna, G. Dellacasa, G.-F. D.  
 262 Betta, M. Ferrero, V. Fadeyev, Z. Galloway, S. Garbolino, H. Grabas, V. Monaco, M. Obertino,  
 263 L. Pancheri, G. Paternoster, A. Rivetti, M. Rolo, R. Sacchi, H. Sadrozinski, A. Seiden, V. Sola,  
 264 A. Solano, A. Staiano, F. Ravera, A. Zatserklyaniy, Tracking in 4 dimensions, Nuclear Instruments  
 265 and Methods in Physics Research Section A: Accelerators, Spectrometers, Detectors and Associated  
 266 Equipment 845 (2017) 47 – 51, proceedings of the Vienna Conference on Instrumentation 2016.  
 267 doi:https://doi.org/10.1016/j.nima.2016.05.078.
- 268 [5] M. Ferrero, R. Arcidiacono, M. Barozzi, M. Boscardin, N. Cartiglia, G. Dalla Betta, Z. Galloway,  
 269 M. Mandurrino, S. Mazza, G. Paternoster, et al., Radiation resistant lgad design, Nuclear Instru-  
 270 ments and Methods in Physics Research Section A: Accelerators, Spectrometers, Detectors and  
 271 Associated Equipment 919 (2019) 16–26.
- 272 [6] V. Sola, R. Arcidiacono, M. Boscardin, N. Cartiglia, G.-F. D. Betta, F. Ficorella, M. Ferrero,  
 273 M. Mandurrino, L. Pancheri, G. Paternoster, A. Staiano, First fbk production of 50  $\mu\text{m}$  ultra-fast  
 274 silicon detectors, Nuclear Instruments and Methods in Physics Research Section A: Accelerators,  
 275 Spectrometers, Detectors and Associated Equipment 924 (2019) 360 – 368. doi:https://doi.org/  
 276 10.1016/j.nima.2018.07.060.
- 277 [7] G. Paternoster, R. Arcidiacono, M. Boscardin, N. Cartiglia, F. Cenna, G. D. Betta, M. Ferrero,  
 278 R. Mulargia, M. Obertino, L. Pancheri, C. Piemonte, V. Sola, Developments and first measurements  
 279 of ultra-fast silicon detectors produced at FBK, Journal of Instrumentation 12 (02) (2017) C02077–  
 280 C02077. doi:10.1088/1748-0221/12/02/c02077.
- 281 [8] M. Andrä, J. Zhang, A. Bergamaschi, R. Barten, C. Borca, G. Borghi, M. Boscardin, P. Busca,  
 282 M. Brückner, N. Cartiglia, S. Chiriotti, G.-F. Dalla Betta, R. Dinapoli, P. Fajardo, M. Ferrero,  
 283 F. Ficorella, E. Fröjd, D. Greiffenberg, T. Huthwelker, C. Lopez-Cuenca, M. Meyer, D. Mezza,  
 284 A. Mozzanica, L. Pancheri, G. Paternoster, S. Redford, M. Ruat, C. Ruder, B. Schmitt, X. Shi,  
 285 V. Sola, D. Thattil, G. Tinti, S. Vetter, Development of low-energy X-ray detectors using LGAD sen-  
 286 sors, Journal of Synchrotron Radiation 26 (4) (2019) 1226–1237. doi:10.1107/S1600577519005393.
- 287 [9] A. Vignati, V. Monaco, A. Attili, N. Cartiglia, M. Donetti, M. F. Mazinani, F. Fausti, M. Ferrero,  
 288 S. Giordanengo, O. H. Ali, et al., Innovative thin silicon detectors for monitoring of therapeutic  
 289 proton beams: preliminary beam tests, Journal of Instrumentation 12 (12) (2017) C12056.
- 290 [10] P. Fernández-Martínez, D. Flores, S. Hidalgo, V. Greco, A. Merlos, G. Pellegrini, D. Quirion,  
 291 Design and fabrication of an optimum peripheral region for low gain avalanche detectors, Nuclear  
 292 Instruments and Methods in Physics Research Section A: Accelerators, Spectrometers, Detectors  
 293 and Associated Equipment 821 (2016) 93 – 100. doi:https://doi.org/10.1016/j.nima.2016.03.  
 294 049.
- 295 [11] V. Sola, R. Arcidiacono, M. Boscardin, G. Borghi, N. Cartiglia, M. Centis Vignali, M. Costa, G. F.  
 296 Dalla Betta, M. Ferrero, M. Mandurrino, L. Pancheri, G. Paternoster, F. Ficorella, A. Staiano,  
 297 F. Siviero, M. Tornago, Interpad optimisation strategies on lgad manufactured at fbk, in: 35th  
 298 RD50 Workshop (CERN), CERN, 2019.
- 299 [12] ATLAS User’s Manual.
- 300 [13] G.-F. D. Betta, L. Pancheri, M. Boscardin, G. Paternoster, C. Piemonte, N. Cartiglia, F. Cenna,  
 301 M. Bruzzi, Design and tcad simulation of double-sided pixelated low gain avalanche detectors,  
 302 Nuclear Instruments and Methods in Physics Research Section A: Accelerators, Spectrometers,  
 303 Detectors and Associated Equipment 796 (2015) 154 – 157. doi:https://doi.org/10.1016/j.  
 304 nima.2015.03.039.
- 305 [14] E. Currás, M. Carulla, M. C. Vignali, J. Duarte-Campderros, M. Fernández, D. Flores, A. García,  
 306 G. Gómez, J. González, S. Hidalgo, et al., Inverse low gain avalanche detectors (ilgads) for precise  
 307 tracking and timing applications, Nuclear Instruments and Methods in Physics Research Section  
 308 A: Accelerators, Spectrometers, Detectors and Associated Equipment 958.
- 309 [15] T. Arnaud, F. Leverd, L. Favennec, C. Perrot, L. Pinzelli, M. Gatefait, N. Cherault, D. Jeanjean,  
 310 J.-P. Carrere, F. Hirigoyen, L. Grant, F. Roy, Pixel-to-pixel isolation by deep trench technology:  
 311 Application to cmos image sensor, 2011.
- 312 [16] C. Piemonte, F. Acerbi, A. Ferri, A. Gola, G. Paternoster, V. Regazzoni, G. Zappala, N. Zorzi,  
 313 Performance of nuv-hd silicon photomultiplier technology, IEEE Transactions on Electron Devices  
 314 63 (3) (2016) 1111–1116. doi:10.1109/TED.2016.2516641.
- 315 [17] C. Dietzinger, P. Iskra, T. Ganka, T. Eggert, L. Höllt, A. Pahlke, N. Miyakawa, M. Fraczek,  
 316 J. Knobloch, F. Wiest, W. Hansch, R. Fojt, Reduction of optical crosstalk in silicon photomultipli-  
 317 ers, in: H. Mohseni, M. H. Agahi, M. Razeghi (Eds.), Biosensing and Nanomedicine V, Vol. 8460,

- 318 International Society for Optics and Photonics, SPIE, 2012, pp. 223 – 231. doi:10.1117/12.930473.  
319 URL <https://doi.org/10.1117/12.930473>
- 320 [18] G. Paternoster, G. Borghi, M. Boscardin, N. Cartiglia, M. Ferrero, F. Ficorella, F. Siviero, A. Gola,  
321 P. Bellutti, Trench-isolated low gain avalanche diodes (ti-lgads), Electron Device Letter, under  
322 review.
- 323 [19] N. Cartiglia, R. Arcidiacono, M. Baselga, R. Bellan, M. Boscardin, F. Cenna, G. D. Betta,  
324 P. Fernandez-Martnez, M. Ferrero, D. Flores, Z. Galloway, V. Greco, S. Hidalgo, F. Marchetto,  
325 V. Monaco, M. Obertino, L. Pancheri, G. Paternoster, A. Picerno, G. Pellegrini, D. Quirion,  
326 F. Ravera, R. Sacchi, H.-W. Sadrozinski, A. Seiden, A. Solano, N. Spencer, Design optimization  
327 of ultra-fast silicon detectors, Nuclear Instruments and Methods in Physics Research Section A: Accelerators,  
328 Spectrometers, Detectors and Associated Equipment 796 (2015) 141 – 148. doi:<https://doi.org/10.1016/j.nima.2015.04.025>.
- 329 [20] G. Giacomini, W. Chen, G. D’Amen, A. Tricoli, Fabrication and performance of ac-coupled lgads,  
330 Journal of Instrumentation 14 (09) (2019) P09004.
- 331 [21] M. Mandurrino, R. Arcidiacono, M. Boscardin, N. Cartiglia, G. F. Dalla Betta, M. Ferrero, F. Fi-  
332 corella, L. Pancheri, G. Paternoster, F. Siviero, M. Tornago, Demonstration of 200-, 100-, and 50-  
333  $\mu$  m pitch resistive ac-coupled silicon detectors (rsd) with 1004d particle tracking, IEEE Electron  
334 Device Letters 40 (11) (2019) 1780–1783. doi:10.1109/LED.2019.2943242.
- 335 [22] M. Mandurrino, R. Arcidiacono, M. Boscardin, N. Cartiglia, G.-F. Dalla Betta, M. Ferrero, F. Fi-  
336 corella, L. Pancheri, G. Paternoster, F. Siviero, et al., Analysis and numerical design of resistive  
337 ac-coupled silicon detectors (rsd) for 4d particle tracking, Nuclear Instruments and Methods in  
338 Physics Research Section A: Accelerators, Spectrometers, Detectors and Associated Equipment 959  
339 (2020) 163479.
- 340 [23] N. Cartiglia, et al., Future silicon trackers, in: Proceedings of the 12th International “Hiroshima”  
341 Symposium (HSTD12) at Hiroshima, Japan, 2020.
- 342 [24] R. Arcidiacono, et al., State-of-the-art and evolution of ufsd sensors design at fbk, in: Proceedings  
343 of the 12th International “Hiroshima” Symposium (HSTD12) at Hiroshima, Japan, 2020.
- 344